

## The Spitzer c2d Survey of Nearby Dense Cores: IV. Revealing the Embedded Cluster in B59

Timothy Y. Brooke<sup>1</sup>, Tracy L. Huard<sup>2</sup>, Tyler L. Bourke<sup>2</sup>, A. C. Adwin Boogert<sup>1,14</sup>, Lori E. Allen<sup>2</sup>, Geoffrey A. Blake<sup>3</sup>, Neal J. Evans, II<sup>4</sup>, Paul M. Harvey<sup>4</sup>, David W. Koerner<sup>5</sup>, Lee G. Mundy<sup>6</sup>, Philip C. Myers<sup>2</sup>, Deborah L. Padgett<sup>7</sup>, Anneila I. Sargent<sup>1</sup>, Karl R. Stapelfeldt<sup>8</sup>, Ewine F. van Dishoeck<sup>9</sup>, Nicholas Chapman<sup>6</sup>, Lucas Cieza<sup>4</sup>, Michael M. Dunham<sup>4</sup>, Shih-Ping Lai<sup>6,12,13</sup>, Alicia Porras<sup>2</sup>, William Spiesman<sup>4</sup>, Peter J. Teuben<sup>6</sup>, Chadwick H. Young<sup>10</sup>, Zahed Wahhaj<sup>5</sup>, Chang Won Lee<sup>11</sup>

### ABSTRACT

---

<sup>1</sup>Astronomy Department, MC 105-24, California Institute of Technology, Pasadena, CA 91125; tyb@astro.caltech.edu

<sup>2</sup>Smithsonian Astrophysical Observatory, 60 Garden Street, Cambridge, MA 02138

<sup>3</sup>Department of Geological and Planetary Sciences, MC 150-21, California Institute of Technology, Pasadena, CA 91125

<sup>4</sup>Department of Astronomy, University of Texas at Austin, 1 University Station C1400, Austin, TX 78712-0259

<sup>5</sup>Department of Physics and Astronomy, Northern Arizona University, Box 6010, Flagstaff, AZ 86011-6010

<sup>6</sup>Department of Astronomy, University of Maryland, College Park, MD 20742

<sup>7</sup>Spitzer Science Center, California Institute of Technology, CA 91125

<sup>8</sup>Jet Propulsion Laboratory, MS 183-900, California Institute of Technology, 4800 Oak Grove Drive, Pasadena, CA 91109

<sup>9</sup>Leiden Observatory, PO Box 9513, 2300 RA Leiden, the Netherlands

<sup>10</sup>Department of Physical Sciences, Nicholls State University, PO Box 2022, Thibodaux, LA 70310

<sup>11</sup>Korea Astronomy and Space Science Institute, 61-1, Hwaam-dong, Yuseong-gu, Daejeon 305-348, South Korea

<sup>12</sup>Institute of Astronomy and Department of Physics, National Tsing Hua University, Hsinchu 30043, Taiwan

<sup>13</sup>Academia Sinica Institute of Astronomy and Astrophysics, P.O. Box 23-141, Taipei 106, Taiwan

<sup>14</sup>NOAO Gemini Science Center, Casilla 603, La Serena, Chile, SA

Infrared images of the dark cloud core B59 were obtained with the *Spitzer Space Telescope* as part of the “Cores to Disks” Legacy Science project. Photometry from 3.6-70  $\mu\text{m}$  indicates at least 20 candidate low-mass young stars near the core, more than doubling the previously known population. Out of this group, 13 are located within  $\sim 0.1$  pc in projection of the molecular gas peak, where a new embedded source is detected. Spectral energy distributions span the range from small excesses above photospheric levels to rising in the mid-infrared. One other embedded object, probably associated with the millimeter source B59-MMS1, with a bolometric luminosity  $L_{\text{bol}} \sim 2 L_{\odot}$ , has extended structure at 3.6 and 4.5  $\mu\text{m}$ , possibly tracing the edges of an outflow cavity. The measured extinction through the central part of the core is  $A_V \gtrsim 45$  mag. The B59 core is producing young stars with a high efficiency.

*Subject headings:* Stars: Pre-main-sequence – Infrared: Stars – ISM: Clouds – Infrared: ISM

## 1. Introduction

One component of the *Spitzer Space Telescope* “Cores to Disks” (*c2d*) Legacy Science program (Evans et al. 2003), is imaging of nearby dark cloud cores at infrared wavelengths ranging from 3.6 to 70  $\mu\text{m}$ . The program takes advantage of *Spitzer’s* high sensitivity (Werner et al. 2004) to survey young stars down to  $\sim 0.001 L_{\odot}$  in these cores. Five large molecular clouds are also being studied by *c2d*. This will allow comparisons to be made between the young star populations in isolated cores and large molecular clouds. *Spitzer’s* high sensitivity in the mid-infrared makes it ideally suited to studying the intermediate stages of star-formation, particularly in dense cores, where dust extinction can obscure the light at visible and near-infrared wavelengths.

This paper presents highlights of the *c2d* observational data of the dark cloud core B59. Though it is a known site of star-formation, there have been relatively few published studies of this core to date and spectral information is apparently lacking for nearly all of the objects discussed here. The *Spitzer* data show the core to be the site of a small cluster of young low-mass stars at a range of evolutionary stages.

## 2. B59

B59 (Barnard 1927; Lynds 1962) is an irregularly-shaped dark cloud roughly  $30' \times 15'$  centered around  $\alpha(\text{J2000}) = 17^{\text{h}} 11.4^{\text{m}}$  and  $\delta(\text{J2000}) = -27^{\circ} 26'$  (Herbig 2005). It sits at the NW end (in galactic coordinates) of the Pipe Nebula, a set of filamentary dark clouds located close to our line of sight to the Galactic Center and above the galactic plane ( $l = 357^{\circ}$ ,  $b = 7.2^{\circ}$  for B59). The nebula also lies close in projection to the Ophiuchus molecular cloud.

The Pipe Nebula was mapped in the  $J = 1 - 0$  lines of  $^{12}\text{CO}$ ,  $^{13}\text{CO}$ , and  $\text{C}^{18}\text{O}$  with the NANTEN telescope using a  $2.7'$  beam (Onishi et al. 1999). They identified 14  $\text{C}^{18}\text{O}$  cores. Molecular outflow emission was detected only towards a single core (their Core 1), within B59. This core has roughly twice the column density of the other cores. The outflow was not clearly identifiable as bipolar, but may be due to two or more different outflows. We will refer to this as the B59 core, and sometimes loosely B59, in this paper.

The distance to B59 is uncertain. The radial velocity of the molecular gas is consistent with a distance similar to the Ophiuchus cloud (Onishi et al. 1999), which is approximately  $d = 125 \pm 25$  pc (de Geus et al. 1989). The distance to the Pipe Nebula was recently estimated by combining extinctions with parallaxes (Lombardi et al. 2006). They obtained  $d = 130_{-20}^{+13}$  pc, where the uncertainties are  $1\sigma$ . This distance is adopted in this paper.

B59 is the only confirmed star-forming region in the Pipe Nebula to date. In addition to the CO outflow(s), there are at least 5  $\text{H}\alpha$  emission-line stars in or near the core: LkH $\alpha$  346 (NW and SE), KW 2, B59-2, and LkH $\alpha$  347 (Cohen & Kuhi 1979; Herbig & Bell 1988; Kohoutek & Wehmeyer 2003; Herbig 2005). Two other  $\text{H}\alpha$  emitters, KK Oph and V359 Oph, are farther from the core center,  $\sim 20'$  and  $\sim 36'$ , or 0.8 and 1.4 pc in projection, but may also be associated with B59 (Herbig 2005).

There are 3 bright IRAS sources in the Point Source Catalog within  $\sim 5.5'$  of the center of the core with spectral energy distributions consistent with young stellar objects, according to the criteria of Lee & Myers (1999): IRAS17079-2719 (associated with LkH $\alpha$  346), IRAS17081-2721, and IRAS17082-2724. Because of the proximity of the emission-line stars and IRAS sources, B59 is categorized by the *c2d* team as a “starred” core. A 1.3 mm continuum survey revealed an additional probable protostellar object, B59-MMS1 (Reipurth et al. 1996), not associated with any of the IRAS sources.

There have been several studies of B59 that have focused on the multiple stars. B59-1 and the emission-line star, LkH $\alpha$  346, are probable triple systems (Chelli et al. 1995; Koresko 2002). Another emission-line star, B59-2, is at least double (Reipurth & Zinnecker

1993; Chelli et al. 1995), and may be triple (Koresko 2002).

### 3. Observations

B59 was observed with the *Spitzer* Infrared Array Camera, IRAC (Fazio et al. 2004), on UT 2004 September 3.9 and 4.2 under Astronomical Observation Requests (AORs) 5131776 and 5132288. The pixel size is  $1.2''$ . Observations at two different epochs allowed identification of asteroids. The IRAC  $3.6\ \mu\text{m}$  and  $5.8\ \mu\text{m}$  arrays observe the same field simultaneously, and the  $4.5\ \mu\text{m}$  and  $8.0\ \mu\text{m}$  arrays a different field. The observations at each epoch consisted of a  $3 \times 4$  map with small overlap regions. For each map there were two dithers of 12-sec exposures, preceded by short high-dynamic-range 0.6-sec exposures (HDR). The HDR observations allowed photometry of sources that saturated at longer integration times. The typical effective observation time was 48 sec. The point-source flux limits for reliable detection were roughly 0.03, 0.03, 0.10, 0.15 mJy at  $3.6$ ,  $4.5$ ,  $5.8$ ,  $8.0\ \mu\text{m}$ , respectively.

Observations of B59 at  $24$  and  $70\ \mu\text{m}$  using the Multiband Infrared Photometer for *Spitzer*, MIPS (Rieke et al. 2004), were obtained on UT 2005 April 6.4 and 7.0 (AORs 9409280 and 9438720). The pixel size is  $2.5''$  at  $24\ \mu\text{m}$  and  $10''$  at  $70\ \mu\text{m}$ . The observations were  $3 \times 3$  photometry maps with 1 cycle of 3 sec observations at  $24\ \mu\text{m}$ , and 3 cycles of 3 sec at  $70\ \mu\text{m}$ . The second epoch was shifted by roughly  $6'$ , to increase coverage at  $70\ \mu\text{m}$ . Typical observation times were 96 sec at  $24\ \mu\text{m}$  and 100 sec at  $70\ \mu\text{m}$ . The point-source flux limits for reliable detection were roughly 0.5 mJy at  $24\ \mu\text{m}$  and 100 mJy at  $70\ \mu\text{m}$ .

The data presented here are from the *Spitzer Science Center's* (SSC) pipeline version S11.4.0. The data were further processed by the *c2d* team to correct artifacts, where possible. This was followed by creation of new mosaics, source photometry up to  $24\ \mu\text{m}$ , bandmerging for the detected wavelengths, and preliminary source typing with extinction estimates. Counterparts in the 2MASS catalog were assigned if found. The procedures are described in Evans et al. (2005). Photometry at  $70\ \mu\text{m}$  was done separately with the SSC's Mopex package, release version 030106 (Makavoz & Marleau 2005).

One exception to these procedures is that three sources in the B59 field saturated at  $24\ \mu\text{m}$  (1, 7, and 11 in Tables 1 and 2) and one source saturated at  $70\ \mu\text{m}$  (source 11). For these sources, photometry was done by fitting the radial profile in the wings with a PSF obtained from an unsaturated bright point source in the field. The flux uncertainty due to this fitting is estimated to be 20 %.

The *Spitzer* photometry is summarized in Table 2. The uncertainties given do not include absolute calibration uncertainties. These are currently estimated by the SSC to be 10 % for IRAC, 10 % for MIPS 24  $\mu\text{m}$ , and 20 % for MIPS 70  $\mu\text{m}$ .

The results in this paper are limited to the region where all IRAC bands and the MIPS 24  $\mu\text{m}$  areas overlap, about 170 arcmin<sup>2</sup>. The MIPS 70 coverage is a subset of this, about 60 % of the area.

## 4. Results

An overview of the young star cluster in B59 is provided by the IRAC 3-color image and the MIPS 24  $\mu\text{m}$  image in Fig. 1a and Fig. 1b. Source 10 (Fig. 1c) is near the peaks in the molecular gas and in the dust extinction, which are discussed below.

Selection of candidate young stars in B59 was based on infrared excesses relative to photospheric colors, after correction for extinction. The excess method is needed because of the absence of any systematic study of the core membership. Correction for extinction is vital due to the high dust column densities toward the core.

As part of its bandmerging, *c2d* checks whether a reddened stellar photosphere can fit the 2MASS and *Spitzer* fluxes at all wavelengths available for each source, within the uncertainties. When this was successful, the source was dropped from consideration as a candidate young star here. Note that some of these may in fact be young stars, though with no detected infrared excesses.

For the remaining sources, which could be young stars, main-sequence or post-main-sequence stars with excesses, or galaxies, we imposed a 24  $\mu\text{m}$  flux lower limit,  $F_\nu(24 \mu\text{m}) > 3 \text{ mJy}$ . This tends to cut out galaxies as the number of galaxies brighter than this is  $\sim 50 \text{ deg}^{-2}$  (Marleau et al. 2004; Papovich et al. 2004), or  $\sim 2$  in our field. (Two of our candidates have no measured 24  $\mu\text{m}$  fluxes due to confusion with nearby sources, but their expected 24  $\mu\text{m}$  fluxes would easily make this cut.)

The galactic background counts toward B59 are less certain. The model of Wainscoat et al. (1992) indicates that for  $F_\nu(24 \mu\text{m}) > 3 \text{ mJy}$ , the number of non-photospheric galactic sources, primarily O-rich and C-rich asymptotic giant branch (AGB) stars, should be small,  $\sim 13 \text{ deg}^{-2}$ , or  $\sim 0.6$  in our field. But models can serve only as a guide for small areas.

Lombardi et al. (2006) identified a population of AGB stars behind the Pipe Nebula

from their location in the 2MASS color-color diagram. These are bright objects, peaking at  $K \sim 7$ , most likely in the galactic bulge. If, as suggested by Lombardi et al., they are similar to the OH/IR star sample of Jiménez-Esteban et al. (2005), then they would be easily detectable at  $24 \mu\text{m}$ ,  $F_\nu(24 \mu\text{m}) \gtrsim 1 \text{ Jy}$ . But they are too few in number to significantly contaminate the young star candidate sample; at  $b = 7.2^\circ$ , there are  $\sim 3 \text{ deg}^{-2}$ , or  $\sim 0.14$  in our field.

To be conservative, we also cut out sources with excesses which appeared close to photospheric levels. We required at least one flux to be a factor  $\sim 4$  higher than the expected photosphere at that wavelength. This eliminated 4 more objects. In doing so, we may have dropped some young stars with weak dust excesses. The motivation is that *c2d* is finding that there are some sources with small IR excesses toward the Serpens cloud that are background AGB stars.

The 20 candidate young stars are listed in Tables 1 and 2. Positions are shown in Fig. 1c. Note that 13 of the objects lie within  $\sim 0.1 \text{ pc}$  in projection of the molecular gas peak (see Fig. 1). We cannot completely eliminate the possibility that some of the proposed young stars are background objects without further data. So we refer to the set as candidate young stars. But some have  $\text{H}\alpha$  in emission (Section 2), and the majority are clustered together close to the center of the core.

For the candidate young stars, we re-evaluated their extinction taking into account the possibility of excess emission in the near-IR. There is no systematic visible photometry of the cloud members, nor is there information on spectral types or effective temperatures for most of the objects. We rely on typical dereddened near-IR colors of young stars.

We assumed that the young stars with all 3 2MASS fluxes in our sample have intrinsic  $\text{JHK}_s$  colors that fall on the locus of the sample of T Tauri stars in Taurus, whose dereddened colors were estimated by Meyer et al. (1997), see Fig. 2. This requires that we are sampling similar spectral types and dust properties as in Taurus. It is difficult to test this without spectroscopic data on the stars. But the assumption has been used for other young clusters, e.g. IC 348 (Muench et al. 2003) and NGC2024 (Haisch et al. 2001), in the absence of better constraints. And Luhman (2004) shows consistency of extinction estimates done this way compared to those obtained from visible spectra for young stars in Cham I.

We adopted the dust extinction law of Indebetouw et al. (2005), which extends from  $1.25\text{-}8.0 \mu\text{m}$ . The  $1.25\text{-}2.2 \mu\text{m}$  extinction of the Pipe Nebula agrees with that of Indebetouw et al. within the uncertainties (Lombardi et al. 2006). Using this dust extinction law, we allowed the young stars to deredden to the locus of  $\text{JHK}_s$  colors of the T Tauri stars, or to the nearest extrapolated point (Fig. 2). Uncertainties from both the data and the locus

envelope are propagated to the extinction estimate (Table 1). By convention, the extinction is given by  $A_V$  in magnitudes, whereas we do not know the extinction law in this region down to visible wavelengths. We only estimate near-infrared values of the extinction, e.g.  $A_K$ . We converted using  $A_V/A_K = 8.9$  from the Rieke & Lebofsky (1985) extinction law, but note that our actual estimates are  $A_K$ . The adopted Indebetouw et al. extinction law appears appropriate for B59 in the JHK<sub>s</sub> bands, as the bright stars in the field follow it (Fig. 2).

For source 8, with only HK<sub>s</sub> data, we deredden to the center of the T Tauri locus, and assign a larger uncertainty. The embedded objects (10, 11) have insufficient near-IR data to correct for extinction by this method.

The dereddened spectral energy distributions (SEDs) are shown in Fig. 3. The 24  $\mu\text{m}$  extinction,  $A_{24}/A_K = 0.24$ , was taken from the Weingartner & Draine (2001) model which fits the Indebetouw et al. points ( $R_V=5.5$ , Case B).

The 2-10  $\mu\text{m}$  or 2-20  $\mu\text{m}$  slope is commonly used to classify young stars in the IR. Following earlier authors (Lada 1987; Wilking et al. 2001; Greene et al. 1994) we define the spectral index as  $\alpha = d\log(\lambda F_\lambda)/d\log\lambda$ . We define the IR spectral classes as follows:  $\alpha \geq 0.3$  is a Class I source,  $0.3 > \alpha \geq -0.3$  a “Flat” type, and  $\alpha < -0.3$  a Class II. These agree with Greene et al. (1994), except that the Class III designation is restricted to sources with practically photospheric slopes after dereddening,  $\alpha \sim -3$  (Kenyon & Hartmann 1995). Because of our selection criteria, we have no Class III sources in the present sample. We use the 2MASS K<sub>s</sub> and IRAC 8  $\mu\text{m}$  fluxes as endpoints, unless noted in Table 2. Slopes and IR class are given in Table 2 for the observed fluxes uncorrected for extinction and with correction for extinction. (Source 1 after correction is on the border of Flat and Class II, but the complete SED indicates it is most like the Flat objects.)

The similarity of the dereddened SEDs to known young stars in other star-forming regions gives us confidence that the  $A_V$  values are reasonable and that all of the objects are young stars. Note in particular (Fig. 3) the strong similarity of most of the Class II sources with  $\alpha \geq -1.6$  to the median Taurus Class II SED from the sample defined by D’Alessio et al. (1999).

#### 4.1. Extinction Map

There are sufficient numbers of background stars detected through the B59 region to

provide an approximate extinction map. The H-K color excess was adopted as a measure of extinction (Lada et al. 1994). This is an effective technique as the spread in H-K colors of main-sequence stars is small ( $\sim 0.3$  mag). We require 2MASS colors at present, so some highly extinguished background stars (for which we could in principle estimate  $A_V$  from *Spitzer* colors alone) could not be used. But there are enough 2MASS sources for a map, and the accuracy and wide use of this method led us to adopt it.

We assumed a mean intrinsic color of H-K = 0.175 for the background stars, which is the mean value for stars in the Pipe Nebula control field of Lombardi et al. (2006), obtained from M. Lombardi (priv. comm.). The conversion to  $A_V$  as described above is  $A_V = 16.8E(\text{H-K})$ , where  $E(\text{H-K})$  is the color excess. The factor 16.8 differs from the commonly used 15.9, due to the adoption of the Indebetouw et al. (2005) near-IR extinction law. Note that the maximum uncertainty in intrinsic color translates into an uncertainty in  $A_V$  for an individual star of 2.5 mag, which is small enough to not affect our results.

The spatial resolution of the extinction map was set by the need for several stars in each spatial bin. This required boxes of size  $\sim 100''$ , and the map was oversampled by a factor 2. The median  $A_V$  in each bin was taken to avoid foreground objects and the scatter gave the uncertainty. The extinction map is shown in Fig. 1d, and interpolated values at the positions of the candidate young stars in Table 1.

The agreement between the total extinction  $A_V$  estimates and those towards individual young stars is not particularly good. Most of the extinction map  $A_V$  values are higher than those derived by dereddening individual objects. This is reasonable since many of the objects could be near the front of the cloud. Two are lower, which may be explained by localized dust.

The measured peak extinction from the background stars is  $A_V \sim 45$  magnitudes, though the true value is likely higher due to the coarse spatial resolution. We estimated the molecular hydrogen column density at the peak using  $N(\text{H}_2) = 9.4 \times 10^{20} A_V$  (Kandori et al. 2005), giving  $N(\text{H}_2) = 4.2 \times 10^{22} \text{ cm}^{-2}$  with a 50 % uncertainty. For the  $\text{C}^{18}\text{O}$  core in B59, Onishi et al. (1999) estimated  $N(\text{H}_2) = 1.5 \times 10^{22} \text{ cm}^{-2}$  from the strength of the  $\text{C}^{18}\text{O}$  line.

## 4.2. Comparison to Gas

In addition to the CO data of Onishi et al. (1999), data for B59 in CS (J=2–1) and  $\text{N}_2\text{H}^+$  (J=1–0) have been obtained at FCRAO with an effective beam size of  $60''$  (C. DeVries,



in preparation). CS integrated intensity contours are shown in Fig. 1e. Source 10 lies close to the CS molecular gas peak. The  $\text{N}_2\text{H}^+$  emission (not shown) is centered near this area, but appears extended NE-SW, i.e. similar to the extinction. No strong, well-organized outflow or infall signatures were detected for either species in these data.

The positions of the CO outflows within our mapped region from Onishi et al. (1999) are marked in Fig. 1e. These are the positions of the peak contours in the red and blue channels defined by those authors. However the large beam size of these observations (2.7') makes detailed comparison to the *Spitzer* sources difficult. It appears that some of the CO outflows are aligned with source 11, rather than source 10 which is closer to the extinction peak (see Sec. 4.4).

The total gas mass in the B59 core estimated from the  $\text{C}^{18}\text{O}$  line is  $\sim 20 M_\odot$  within a radius of  $\sim 0.15$  pc (Onishi et al. 1999, both adjusted for the different assumed distances).

The total gas mass in the core can also be estimated from the dust extinction of background stars under the assumption that dust within the core provides most of the extinction. The conversion from  $A_V$  to  $N(\text{H}_2)$  for typical interstellar dust is given above. For a standard cloud composition with mean atomic weight per H atom,  $\mu = 1.37$  (Lombardi et al. 2006), the total core mass integrated within the confines of the  $\text{C}^{18}\text{O}$  core is  $M_{\text{core}} = 25 \pm 1 M_\odot$ , where the uncertainty does not include the distance uncertainty.

These two estimates of core gas mass are in good agreement, considering the different spatial resolutions. Some freeze-out of CO is probable in the dense regions. Although solid CO has not yet been observed toward B59, sources near the center of the core have deep solid  $\text{H}_2\text{O}$  and  $\text{CO}_2$  bands (A. Boogert, in prep.).

### 4.3. Class 0/I and I Sources and Bolometric Luminosities

Based on their SED's there are two deeply embedded objects near the center of the B59 core. Source 11 = 2MASSJ17112317-2724315 (hereafter 2MASS171123) lies  $\sim 15''$  E of the quoted position of the 1.3 mm source B59-MMS1 observed with a  $22''$  HPBW beam (Reipurth et al., 1996) and the two are probably the same. The total 1.3mm flux integrated to the  $8\sigma$  contour was 725 mJy. It was recently detected at  $350 \mu\text{m}$  with the SHARCII bolometer array at the Caltech Submillimeter Observatory (Wu et al. 2006, submitted to ApJ). The flux in a  $40''$  diameter aperture is  $45.2 \pm 8.0$  Jy.

With most of the SED for this source in hand (Fig. 4), we estimated the bolometric

luminosity,  $L_{\text{bol}} = 2.2 \pm 0.3 L_{\odot}$ , the bolometric temperature,  $T_{\text{bol}} = 70 \pm 10$  K (Myers & Ladd 1993), and the ratio of sub-mm ( $\gtrsim 350 \mu\text{m}$ ) to bolometric luminosity ( $L_{\text{smm}}/L_{\text{bol}} = 0.03 \pm 0.01$ ). The uncertainty in luminosity does not include the distance uncertainty.

In addition to the Class I-III spectral classes for young stars discussed above, a fourth class, Class 0, is used to define cold sources. Two common criteria for a Class 0 source are that  $T_{\text{bol}} < 70$  K and  $L_{\text{smm}}/L_{\text{bol}} > 0.5 \%$  (André et al. 2000).

2MASS171123 lies somewhere near the border of this definition, so may be described as a Class 0/I source.

As noted by Young et al. (2004) and others, heating of dust by the interstellar radiation field may contribute to the fluxes of low-luminosity protostars longward of  $\sim 100 \mu\text{m}$ . Thus high values of  $L_{\text{smm}}/L_{\text{bol}}$  may be common for low-luminosity protostars at some point during their lifetime, and some revision of this criterion may be needed.

The other nominal Class I object, source 10, is close to the gas and dust extinction peaks. It lacks a complete SED at present, but appears spectrally similar to source 11 in the mid-IR, so we estimate a bolometric luminosity by scaling,  $L_{\text{bol}} \sim 0.6 L_{\odot}$ , but this is only a crude estimate. We will leave its designation as Class I for the present time, pending mm and sub-mm observations.

We are not able to determine directly the final stellar masses for these two Class 0/I or I sources. The models of Myers et al. (1998) suggest that source 11 and source 10 will evolve to form stars with 0.5 and 0.3  $M_{\odot}$ , and have ages of  $t \sim 0.1 - 0.2$  Myr.

It is probable that one or both of the embedded sources near the center of the core we detect with *Spitzer* are the youngest objects and drive the CO outflows seen by Onishi et al. (1999). Further study of these objects and their possible disks and outflows with IR and mm and sub-mm interferometry is needed.

Bolometric luminosities (Table 2) for the rest of the candidate young stars were estimated as follows. For the Class II sources with  $\alpha < -1.6$ , late-type photospheres were fitted to the dereddened J-band fluxes. The IR excesses add only marginally to the bolometric luminosity. For the Class II sources with  $\alpha \geq -1.6$ , we used the absolute J band flux vs. bolometric luminosity relation from Greene et al. (1994). For the Flat sources, we have no good estimate; only lower limits were obtained by integration under the observed fluxes.

Estimated bolometric luminosities for the Class II sources range from 0.1-1.8  $L_{\odot}$ . The central stars provide the bulk of the contribution to the bolometric luminosity for these objects. Stellar evolutionary models (e.g. D’Antona & Mazzitelli 1994; Siess et al. 2000) show that for plausible ages of  $t = 0.5 - 1.0$  Myr, the stellar masses are  $\sim 0.1 - 0.9 M_{\odot}$ ,

corresponding to mid G to late M dwarfs. There are no clear brown dwarf candidates in the present sample.

#### 4.4. Extended Structure around 2MASS171123

The Class 0/I source 2MASS171123 has extended structure at 3.6 and 4.5  $\mu\text{m}$  (Fig. 5), extending out  $\gtrsim 30''$  (0.02 pc) to the NE and SE. There is a trace of extension at 5.8  $\mu\text{m}$  also. These arcs may trace the edges of an outflow cavity in reflected light. The morphology suggests a disk inclined to the line of sight. A possible third extension to the W is confused with a superposed background source.

The apparent outflow axis defined by the E lobes is  $\sim 50^\circ$  E of N. This lines up with some of the CO outflow peaks (Onishi et al. 1999; see Fig. 1e). But the low spatial resolution of the CO data makes a firm identification of specific outflows with this source difficult.

The arcs are unlikely to be due to  $\text{H}_2$  emission, because the *Spitzer* IRS spectrum of the object shows no evidence of  $\text{H}_2$  emission lines at longer wavelengths (A. Boogert, in preparation).

#### 4.5. Extended Emission

The *Spitzer* images of B59 show two kinds of extended emission above the background zodiacal emission.

First is the red (8.0  $\mu\text{m}$ ) emission seen most clearly in the NW area of Fig. 1f, roughly 0.8 MJy/sr above background. This is due to galactic cirrus dust emission. The same structure is seen in the IRAC 5.8  $\mu\text{m}$  band near the detection limit (not shown). The band ratio is  $I(5.8)/I(8) \approx 0.25$ . The emission at 24  $\mu\text{m}$  also broadly traces the same area, with  $I(24)/I(8) \approx 0.4$ . These flux ratios are in the range expected for galactic cirrus (e.g. Reach et al. 2004), with the 8  $\mu\text{m}$  flux due mostly to the emission in the strong aromatic hydrocarbon bands at 7.7 and 8.6  $\mu\text{m}$ .

The second extended structure is more interesting: a wide greenish glow centered on the core, due to emission in the IRAC 4.5  $\mu\text{m}$  band with a contribution from the blue 3.6  $\mu\text{m}$  band. This emission is just visible in Fig. 1f (it may be easier to see in the online

version). The band ratio is roughly  $I(3.6)/I(4.5) = 0.75$ . This emission is not detected at longer wavelengths. The coincidence of the emission with the cloud core is an indication that this is due to scattered galactic light, sometimes called cloudshine (Foster & Goodman 2006).

Cloudshine has been seen in many dense cloud cores at visible (Witt & Stephens 1974) and near-IR wavelengths (Lehtinen & Mattila 1996; Nakajima et al. 2003; Foster & Goodman 2006). The JHK data of Foster & Goodman (2006) have been used to study dust structure on sub-arcsecond scales (Padoan et al. 2006). It is reasonable to expect cloudshine at longer wavelengths as well, though typical interstellar grains will have decreased scattering efficiency at longer wavelengths. Longer wavelengths will in principle penetrate deeper into the cloud, but the visibility will depend on the sensitivity of the observations and the strength of the ambient galactic light.

This explanation is favored over  $H_2$  line emission because of the lack of an obvious jet or shock morphology, and because no  $H_2$  lines are seen in the IRS spectrum of source 10 (A. Boogert, in preparation).

## 5. Discussion

The *Spitzer* data reveal the dark cloud core B59 to be a region of active low-mass star formation containing a small cluster of young stars at different evolutionary stages. Some authors (e.g. Lada & Lada 2003) prefer to reserve the word cluster for groups of  $\geq 35$  objects, but we use the term in a general sense here. Some notable aspects and limitations of the *Spitzer* observations are discussed in this section.

*Completeness for Weak Excesses*– The sensitivity of this analysis to young stars with weak dust excesses is limited by the  $24 \mu\text{m}$  flux cutoff of 3 mJy. A hypothetical young star at  $A_V = 10$  with a factor 4 excess at  $24 \mu\text{m}$  would not make the cut if it’s unextincted photosphere had a flux below 1 mJy. For a main-sequence object at  $d = 130 \text{ pc}$ , this corresponds to a mid-K dwarf. For a more likely age of  $t \sim 1 \text{ Myr}$ , this corresponds to an object that will become roughly a mid-M dwarf (Baraffe et al. 2002). Later spectral types make the cut if they have more substantial excesses. So the sample defined here may be incomplete in Class II for late spectral types with weak excesses.

*IRAC Color-Color Plot*– Many *Spitzer* studies of young stars are possible with IRAC alone, e.g. Hartmann et al. (2005). Fig. 6 shows an IRAC color-color plot for the candidate

young stars in B59 for comparison to IRAC studies of other star-forming regions. The colors plotted are as observed, though the IR spectral classes indicated are after correction for extinction, where possible. Table 2 has the IR spectral classes before correction for extinction. The adopted magnitude zero points were 278 Jy ( $3.6 \mu\text{m}$ ), 180 Jy ( $4.5 \mu\text{m}$ ), 117 Jy ( $5.8 \mu\text{m}$ ), and 63.1 Jy ( $8.0 \mu\text{m}$ ).

*Disk Properties and Age*– We have as yet no direct measure of age (e.g. Li absorption lines) for any of the candidate young stars. The IR spectral classes give a rough measure of age, with Class I being the youngest and Class III the oldest (Kenyon & Hartmann 1995).

Many authors use a two-class definition for the IR spectral classes:  $\alpha > 0$  for Class I,  $\alpha < 0$  for Class II. For comparison in the next paragraph, B59 has a two-class Class I to Class II ratio of 3:17, or 18 %.

The two-class Class I/Class II ratio of 18 % can be compared to *Spitzer* results on other young clusters: 17-34 % for the Tr 37 globule ( $t \sim 1$  Myr, Sicilia-Aguilar et al. (2006); Reach et al. (2004)); 25 % for NGC 7129 ( $t \sim 1$  Myr, Muzerolle et al. (2004)); and 33 % for the Spokes cluster in NGC 2264 ( $t \sim 0.5$  Myr, Teixeira et al. (2006)). For two clusters in Perseus, Jorgensen et al. (2006) find: 29 % for NGC1333 ( $t \lesssim 1$  My) and 15 % for the older IC348 ( $t \sim 2$  Myr).

The above comparisons should be taken only as suggestive due to several factors: some studies do no extinction corrections; there are different sensitivities for different young star selection techniques; and sensitivities differ because of different cloud distances.

We can also use an argument based on the predicted lifetimes of embedded and T Tauri phases (Myers et al. 1987; Kenyon et al. 1990) to estimate the onset of star-formation in B59. For a fixed star-formation rate of objects which evolve from Class I ( $t_{life} \sim 10^5$  yr) to Class II ( $t_{life} \sim 10^6$  yr) the relative numbers suggest an age of  $\sim 0.7 \times 10^6$  yr. Clearly the number of objects in each bin in B59 makes this argument only approximate. And we have neglected potentially important factors, e.g. the effect of the stellar environment on disk lifetimes.

Multiplicity also complicates the interpretation. The suspected young star pair resolved with *Spitzer*, LkH $\alpha$  346 NW and SE (itself a probable double), have very different SEDs (our IR spectral classes are Flat and Class II, respectively). If coeval, the simple model sketched above is wrong. In addition, the frequency of disks may be a function of spectral type, as indicated by a recent *Spitzer* study of IC348 (Lada et al. 2006).

In Fig. 3, we compared the SEDs of the B59 Class II objects with  $\alpha \geq -1.6$  to a median of a sample of mostly Class II objects in Taurus (D’Alessio et al. 1999). The Taurus SED

can be reasonably fitted by optically thick disks with flaring at large radii (D’Alessio et al. 1999). With time, disks are expected to clear from inside-out due to dust coagulation into planetesimals and dynamical clearing. Evidence for such transition disks has recently been shown for IC 348 ( $t \sim 2$  Myr, Lada et al.(2006)) and Tr 37 ( $t \sim 4$  Myr, Sicilia-Aguilar et al. (2006)). The fact that most of the SEDs of the Class II sources with  $\alpha \geq -1.6$  in B59 are similar to the Taurus SED suggests a comparable age for the cloud,  $t \sim 0.7$  Myr (Kenyon & Hartmann 1995).

We see no clear “transition objects”, such as CoKu Tau/4 (Hartmann et al. 2005), those which have very little excess in the IRAC bands, then a large  $24 \mu\text{m}$  excess.

These comparisons taken together suggest an age for B59 of between 0.5 and 1 Myr. Deep optical and near-IR photometric and spectroscopic surveys of the cloud are needed to ensure the membership and measure more accurate age indicators.

*Star Formation in B59*– To date, B59 is the only known star-forming cloud in the Pipe Nebula. Onishi et al. (1999) suggest that this is due to its proximity to the B0 star  $\tau$  Oph, with a stellar wind having triggered star formation.

It is notable that the star formation efficiency of B59 is relatively high. Taking just the objects near the core, there are 13 young stars in  $\sim 25 M_{\odot}$  of dense gas, or  $0.52 M_{\odot}^{-1}$ . Of the 179  $\text{C}^{18}\text{O}$  cores in nearby star-forming regions covered in the NANTEN survey, only a few have a comparable efficiency (Tachihara et al. 2002, and references therein). By way of contrast, the Taurus cloud as a whole has roughly 200 young stars in  $\sim 10^4 M_{\odot}$  of gas (Kenyon & Hartmann 1995; Lada et al. 1993).

Assuming an average mass for the young stars in B59 of  $0.5 M_{\odot}$ , the star formation efficiency as defined by Lada & Lada (2003),  $M_{star}/(M_{star}+M_{gas}) = 0.21$ , close to the maximum of  $\sim 0.3$  seen in their survey of young stellar clusters.

The surface density of young stars in the inner core region of B59 is  $\sim 200 \text{ pc}^{-2}$ . This is a lower limit to the young star population as we require infrared excess for inclusion. The surface density is greater than those of 90 % of the young clusters tabulated in Lada & Lada (2003), though not as high as much more massive clusters such as S106 and the Trapezium. However, the B59 core is smaller than most of the Lada & Lada sample. Comparison to the NANTEN core sample cited above again reveals only a few with comparable young-star surface density. Recent *c2d* observations of another small cluster, L1251B, give a comparable stellar density to B59 (Lee et al. 2006).

Compared to all of the cores in the NANTEN CO survey (Tachihara et al. 2002), B59 is notable for its high gas column density, higher than nearly all of the starless and single-

star-forming cores, but similar to their cluster-forming cores ( $\gtrsim 10$  stars), consistent with our survey findings of a small cluster in formation.

As noted by Lada & Lada (2003), our inventory of young, embedded star clusters, even within a few hundred parsecs, is still incomplete. Data from the *Spitzer* Space Telescope are helping to complete that inventory.

## 6. Summary

1) At least 20 candidate young stars in the B59 core have been identified from infrared excesses in *Spitzer* 3.6-70  $\mu\text{m}$  observations. Spectral energy distributions including corrections for extinction are presented. They range from small excesses above photospheric levels to rising in the mid-infrared. The SEDs of most of the Class II spectral types with spectral index  $\alpha \geq -1.6$  are similar to the SED of the Class II sample in the Taurus cloud of D'Alessio et al. (1999).

2) Thirteen of the young star candidates are located within  $\sim 0.1$  pc in projection of the molecular gas and dust extinction peak. Two Class 0/I or I sources are identified. One, 2MASSJ17112317, probably associated with the millimeter source B59-MMS1, with a bolometric luminosity  $L_{\text{bol}} \sim 2 L_{\odot}$ , has extended structure at 3.6 and 4.5  $\mu\text{m}$ , possibly tracing the edges of an outflow cavity. The other is near the molecular gas and extinction peak and previously unrecognized.

3) The measured extinction through the central part of the B59 core is  $A_V \gtrsim 45$  mag. There are extended infrared emission regions due to galactic cirrus emission and scattered galactic light.

4) Although further study of the young star population in B59 is needed, the data to date suggest the B59 core is producing young stars with high efficiency.

We thank M. Lombardi (ESO) for assistance, C. DeVries (CSU Stanislaus) for making molecular line data available prior to publication, and R. Gutermuth (CfA) for display scripts. We thank the referee whose comments improved the paper. This work is based on observations made with the *Spitzer Space Telescope*, which is operated by the Jet Propulsion Laboratory, California Institute of Technology, under NASA contract 1407. Support for this work, part of the Spitzer Space Telescope Legacy Science Program, was provided by NASA through contract numbers 1224608, 1230779, and 1230780 issued by the Jet Propulsion

Laboratory, California Institute of Technology, under NASA contract 1407. Astrochemistry in Leiden is supported by a NWO Spinoza grant and a NOVA grant. CWL acknowledges support from KOSEFF grant R01-2003-000-10513-0. This publication makes use of data products from the Two Micron All Sky Survey, which is a joint project of the University of Massachusetts and the Infrared Processing and Analysis Center/California Institute of Technology, funded by NASA and NSF. This research has made use of the SIMBAD database, operated at CDS, Strasbourg, France.



## REFERENCES

- André, P., Ward-Thompson, D., & Barsony, M. 2000, in *Protostars and Planets IV*, ed. V. Mannings, A.P. Boss, & S.S. Russell (Tucson:Univ. Arizona Press), 59
- Baraffe, I., Chabrier, G., Allard, F. & Hauschildt, P. 2002, *A&A*, 382, 563
- Barnard, E.E. 1927, *Catalogue of Dark Objects in the Sky*, Carnegie Institute of Washington Publ. 247, Part I
- Bessell, M.S., & Brett, J.M. 1988, *PASP*, 100, 1134
- Carpenter, J.M. 2001, *AJ*, 121, 2851
- Chelli, A., Cruz-Gonzalez, I., & Reipurth, B. 1995, *A&AS*, 114, 135
- Cohen, M., & Kuhl, L.V. *ApJS*, 41, 743
- de Geus, E.J., de Zeeuw, P.T., & Lub, J. 1989, *A&A*, 216, 44
- D'Alessio, P., Calvet, N., Hartmann, L., Lizano, S., & Canto, J. 1999, *ApJ*, 527, 893
- D'Antona, F., & Mazzitelli, I. 1994, *ApJS*, 90, 467
- Evans, N. J., et al. 2003, *PASP*, 115, 965
- Evans, N. J., et al. 2005, *Delivery of Data from the c2d Legacy Project: IRAC and MIPS (Pasadena, SSC)*, <http://ssc.spitzer.caltech.edu/legacy/original.html>
- Fazio, G.G., et al. 2004, *ApJS*, 154, 10
- Foster, J.B. & Goodman, A.A. 2006, *ApJ*, 636, L105
- Greene, T.P., Wilking, B.A., André, P., Young, E.T., & Lada, C.J. 1994, *ApJ*, 434, 614
- Haisch, K.E., Lada, E.A., Pina, R.K., Telesco, C.M., & Lada, C.J. 2001, *ApJ*, 121, 1512
- Hartmann, L. et al. 2005, *ApJ*, 629, 881
- Herbig, G.H. 2005, *AJ*, 130, 815
- Herbig, G.H., & Bell, K.R. 1988, *Lick Obs. Bull.* 1111
- Indebetouw, R., et al. 2005, *ApJ*, 619, 931

- Jiménez-Esteban, F.M., Agudo-Mérida, L., Engels, D., & García-Lario, P. 2005, *A&A*, 431, 779
- Jorgensen, J., et al. 2006, *ApJ*, 645, 1246
- Kandori, R., et al. 2005, *AJ*, 130, 2166
- Kenyon, S.J., & Hartmann, L. 1995, *ApJS*, 101, 117
- Kenyon, S.J., Hartmann, L.W., Strom, K.M., & Strom, S.E. 1990, *AJ*, 99, 869
- Kohoutek, L., & Wehmeyer, R. 2003, *Astron. Nachr.* 324, 437
- Koresko, C.D. 2002, *AJ*, 124, 1082
- Lada, C.J. 1987, in *Star Forming Regions*, IAU Symp. 115, ed. M. Peimbert & J. Jugaku (Dordrecht: Reidel), 1
- Lada, C.J. & Lada, E.A. 2003, *ARA&A*, 41, 57
- Lada, C.J., Lada, E.A., Clemens, D.P., & Bally, J. 1994, *ApJ*, 429, 694
- Lada, C.J. et al. 2006, *ApJ*, 131, 1574
- Lada, E.A., Strom, K.M., & Myers, P.C. 1993, in *Protostars and Planets III*, ed. E.H. Levy & J.I. Lunine (Tucson: Univ. Arizona Press), 245
- Lee, C.W. & Myers, P.C. 1999, *ApJS*, 123, 233
- Lee, J.-E. et al. 2006, *ApJ*, 648, 491
- Lehtinen, K., & Mattila, K. 1996, *A&A*, 309, 570
- Lombardi, M., Alves, J., & Lada, C.J. 2006, *A&A*, 454, 781
- Luhman, K.L. 2004, *ApJ*, 602, 816
- Lynds, B.T. 1962, *ApJS*, 7, 1
- Makavoz, D. & Marleau, F.R., et al. 2005, *PASP*, 117, 113
- Marleau, F.R., et al. 2004, *ApJS*, 154, 66
- Meyer, M.R., Calvet, N., & Hillenbrand, L.A. 1997, *AJ*, 114, 288
- Myers, P.C., Adams, F.C., Chen, H., & Schaff, E. 1998, *ApJ*, 492, 703

- Myers, P.C., Fuller, G.A., Mathieu, R.D., Beichman, C.A., Benson, P.J., Schild, R.E., & Emerson, J.P. 1987, *ApJ*, 319, 340
- Myers, P.C., & Ladd, E.F. 1993, *ApJ*, 413, L47
- Muench, A.A., et al. 2003, *AJ*, 125, 2029
- Muzerolle, J., et al. 2004, *ApJS*, 154, 379
- Nakajima, Y., et al. 2003, *AJ*, 125, 1407
- Onishi, T., Kawamura, A., Abe, R., Yamaguchi, N., Saito, H., Moriguchi, Y., Mizuno, A., Ogawa, H., & Fukui, Y. 1999, *PASJ*, 51, 871
- Padoan, P., Juvela, M., & Pelkonen, V.-M. 2006, *ApJ*, 636, L101
- Papovich, C., et al. 2004, *ApJS*, 154, 70
- Reach, W.T., et al. 2004, *ApJS*, 154, 385
- Reipurth, B., Nyman, L.Å., & Chini, R. 1996, *A&A*, 314, 258
- Reipurth, B., & Zinnecker, H. 1993, *A&A*, 278, 81
- Rieke, G.H., & Lebofsky, M.J. 1985, *ApJ*, 288, 618
- Rieke, G.H., et al. 2004, *ApJS*, 154, 25
- Sicilia-Aguilar, A., et al. 2006, *ApJ*, 638, 897
- Siess, L., Dufour, E., & Forestini, M. 2000, *A&A*, 358, 593
- Tachihara, K., Onishi, T., Mizuno, A., & Fukui, Y. 2002, *A&A*, 385, 909
- Teixeira, P.S., et al. 2006, *ApJ*, 636, L45
- Wainscoat, R.J., Cohen, M.J., Volk, K., Walker, H.J., & Schwartz, D.E. 1992, *ApJS*, 83, 111
- Weingartner, J.C., & Draine, B.T. 2001, *ApJ*, 548, 296
- Werner, M.W., et al. 2004, *ApJS*, 154, 1
- Willing, B.A., Bontemps, S., Schuler, R.E., Greene, T.P., & André, P. 2001, *ApJ*, 551, 357
- Witt, A.N., & Stephens, T.C. 1974, *AJ*, 79, 948
- Young, C.H., et al. 2004, *ApJS*, 154, 396



Fig 1 – Multiwavelength views of the B59 region. *a)* 3-color composite in IRAC filters: 3.6  $\mu\text{m}$  (*blue*), 4.5  $\mu\text{m}$  (*green*), and 8.0  $\mu\text{m}$  (*red*). *b)* MIPS 24  $\mu\text{m}$  image revealing the young star cluster. Nonstar-like features seen  $\pm 2'$  roughly N and S of bright objects are artifacts due to latent images. *c)* Source ID key for candidate young stars from Table 1, with IRAC 4.5  $\mu\text{m}$  image in background. Young star IR spectral classes have the following symbols: Class I (*circle*), Flat (*square*), and Class II (*diamond*). Scale bar is for adopted distance of  $d = 130$  pc. *d)* Estimated  $A_V$  from 2MASS data with Digital Sky Survey Red image. Extinction map has resolution  $\sim 100''$  and contours at  $A_V = 10, 14, 19, 30,$  and  $45$  mag. *e)* MIPS 24  $\mu\text{m}$  image with CS (J=2-1) integrated intensity contours with a  $60''$  beam from C. DeVries (priv. comm.). Contours are at 0.36, 0.50, 0.70, and 0.85 K  $\text{kms}^{-1}$ . CO red outflow (*dark x*), and CO blue outflow peaks (*dark crosses*) are from Onishi et al. (1999). These are the peak positions of the integrated line flux in red and blue channels. A third blue CO outflow peak is off the map to the SE. *f)* Same as (*a*) but stretched to show extended emission.

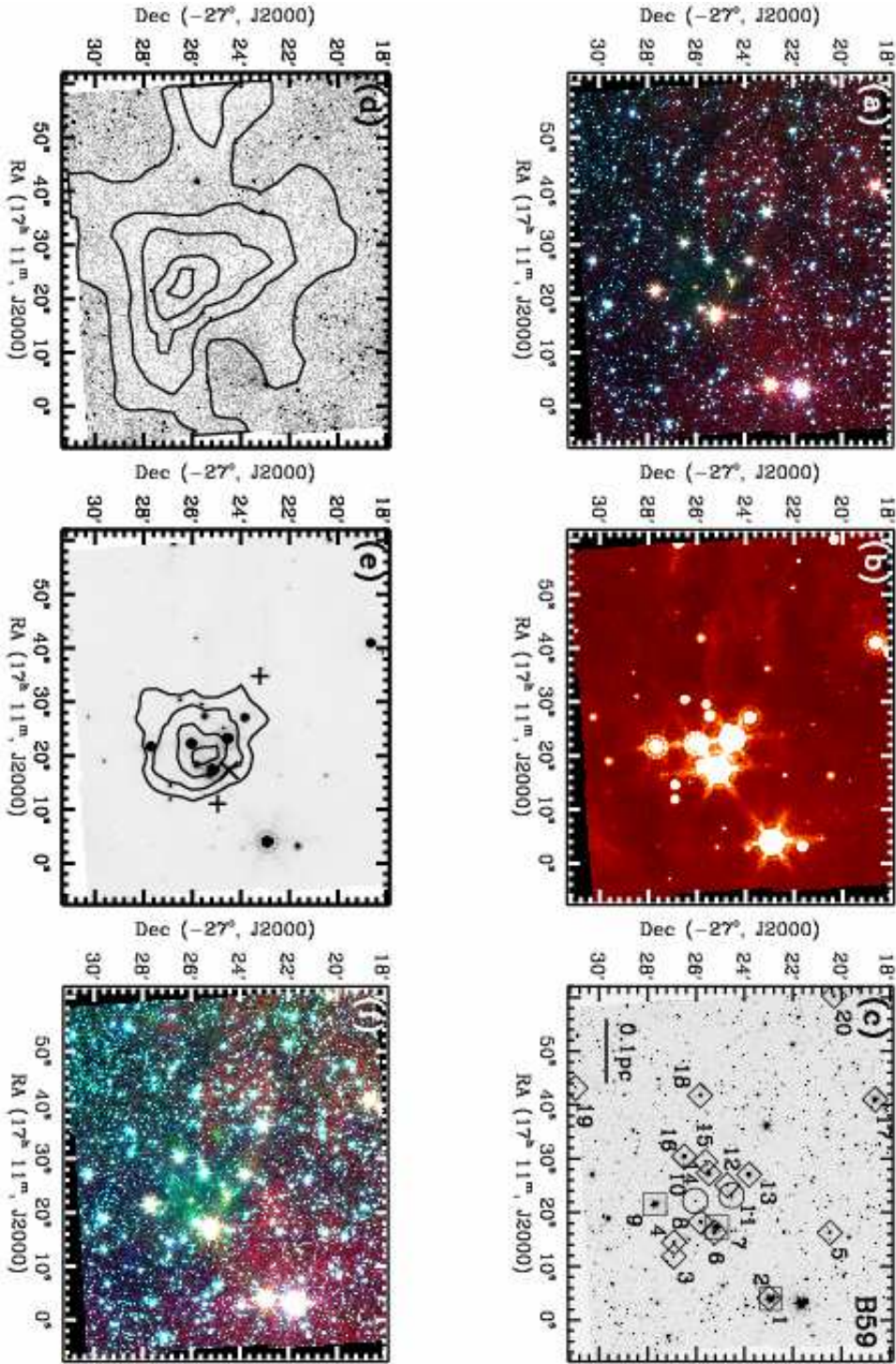


Fig. 1.—

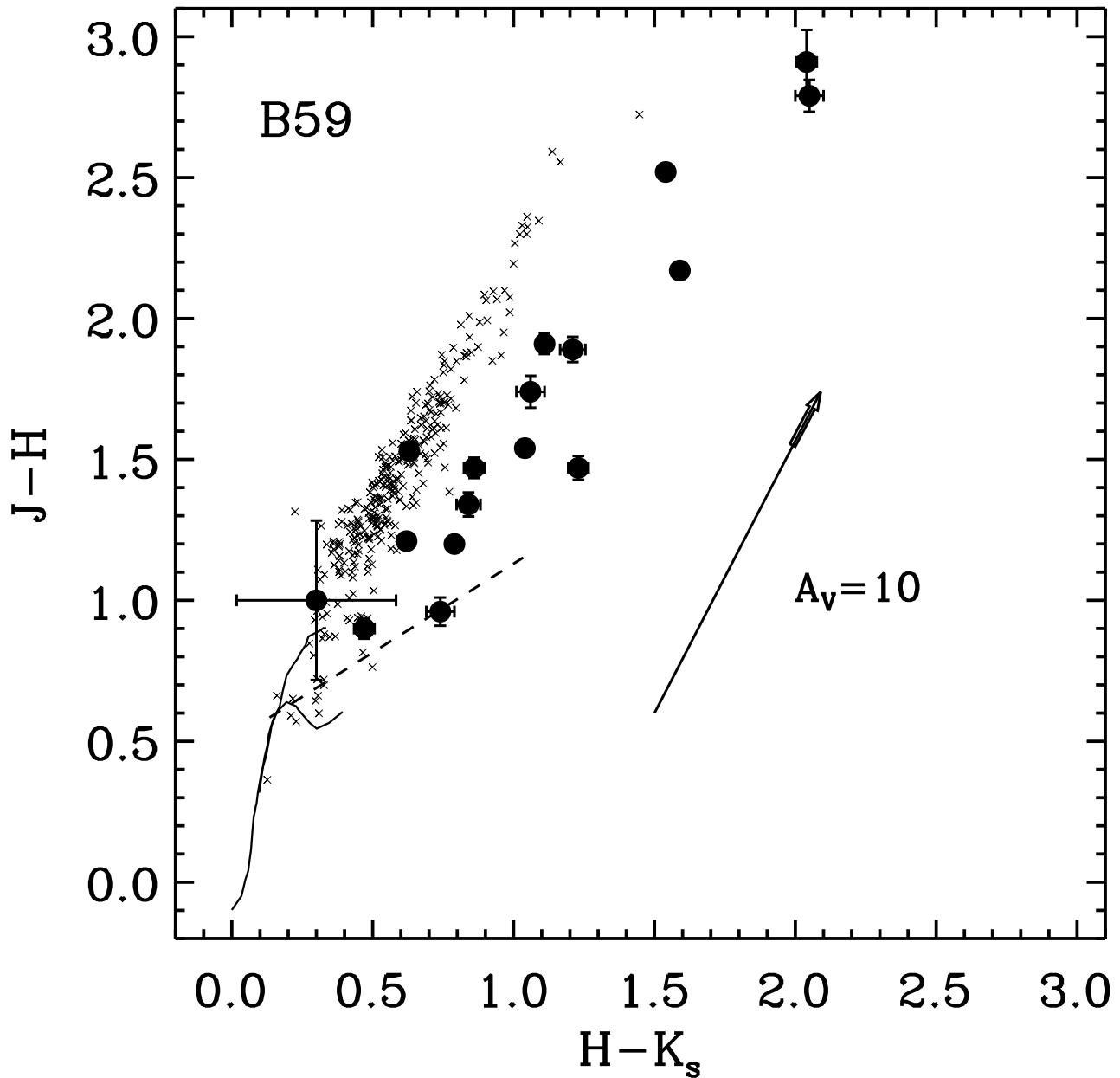


Fig. 2.— 2MASS JHK<sub>s</sub> fluxes of candidate young stars in B59 (*filled circles*) and objects with J flux  $\gtrsim 2.5$  mJy and classified as stars by *c2d* (*small x's*). Main sequence and giants from Bessell & Brett (1988) are the *solid lines*, and the Taurus T Tauri main locus from Meyer et al. (1997) is the *dashed line*. Both are converted to the 2MASS system using Carpenter (2000). The reddening arrow shows the adopted extinction law (Indebetouw et al., 2005) converted to  $A_V$  (see text) and with  $A_V = 10$  mags.

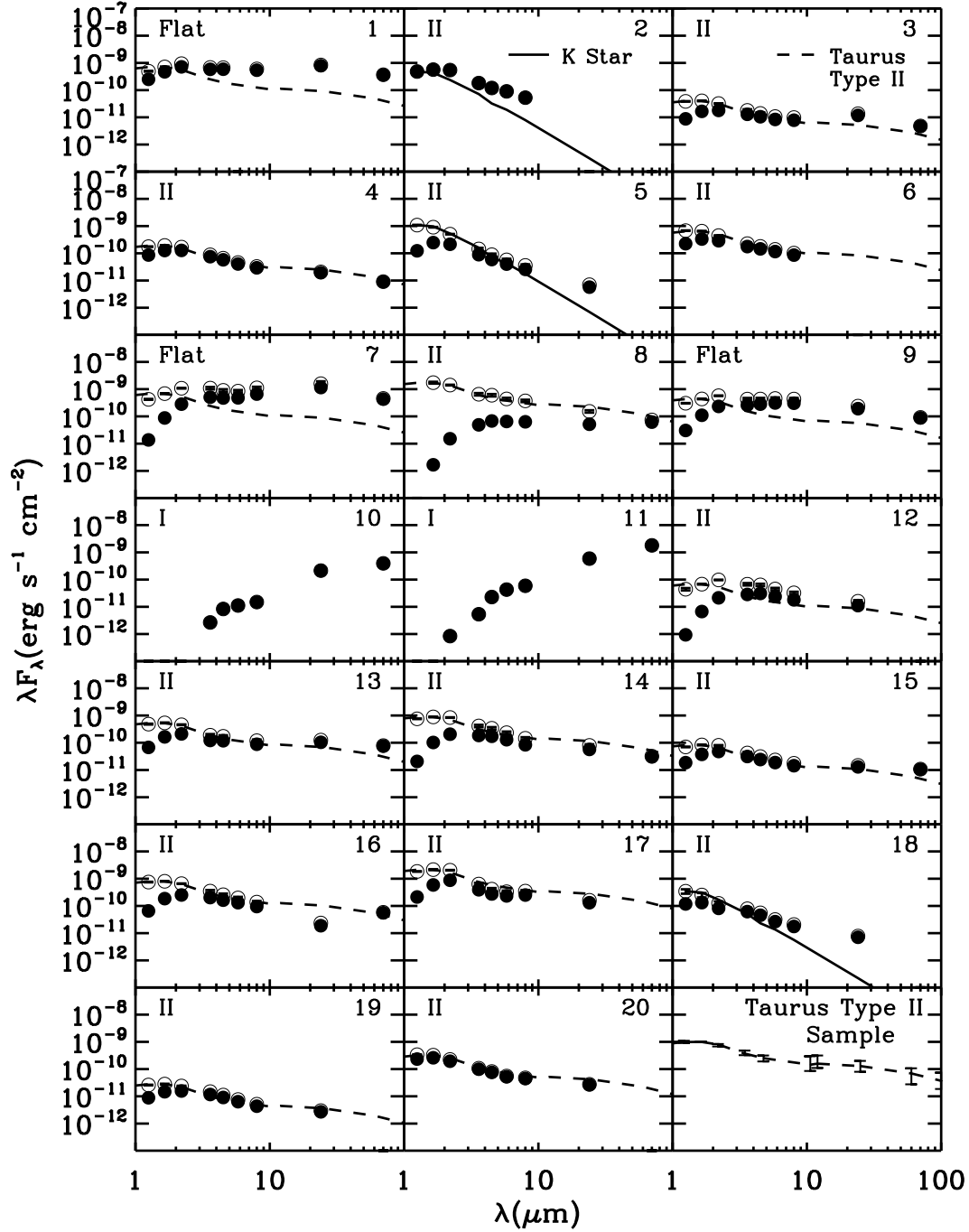


Fig. 3.— Spectral energy distributions (SEDs) of the candidate young stars in B59 as observed (*filled circles*) and after correction for extinction as described in text (*open circles*). Error bars, including absolute calibration uncertainties, are shown, but are smaller than the symbols. In each object panel, the source number (Table 1) is in the upper right and the IR spectral class after correction for extinction, where possible, is in the upper left. The two Class I sources are not corrected for extinction. For the Flat and Class II sources with  $\alpha \geq -1.6$ , the median Class II SED of Taurus sources (*lower right box*, D’Alessio et al. 1999) scaled at H (1.65  $\mu\text{m}$ ), is plotted for comparison (*short dashed lines*). Class II sources with  $\alpha < -1.6$  have a K7 photosphere scaled at J(1.25  $\mu\text{m}$ ) (*solid lines*).



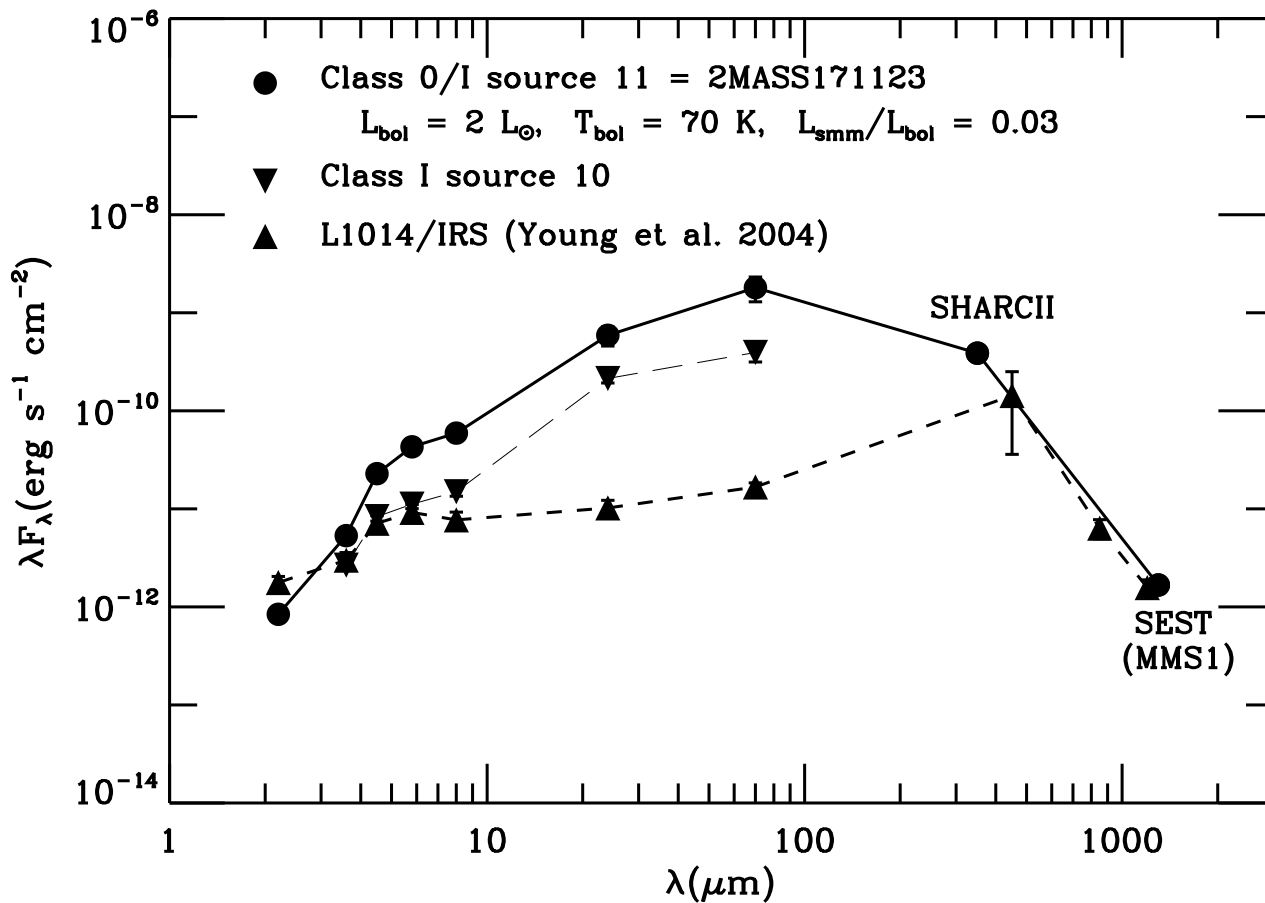


Fig. 4.— Spectral energy distributions of the candidate Class 0/I or I protostars in B59, compared to the infrared source in L1014. For 2MASS171123, the SHARCII 350  $\mu\text{m}$  data point is from Wu et al. (2006, submitted to ApJ). SEST 1.3mm data point of MMS1 is from Reipurth et al. (1996). See text for details.

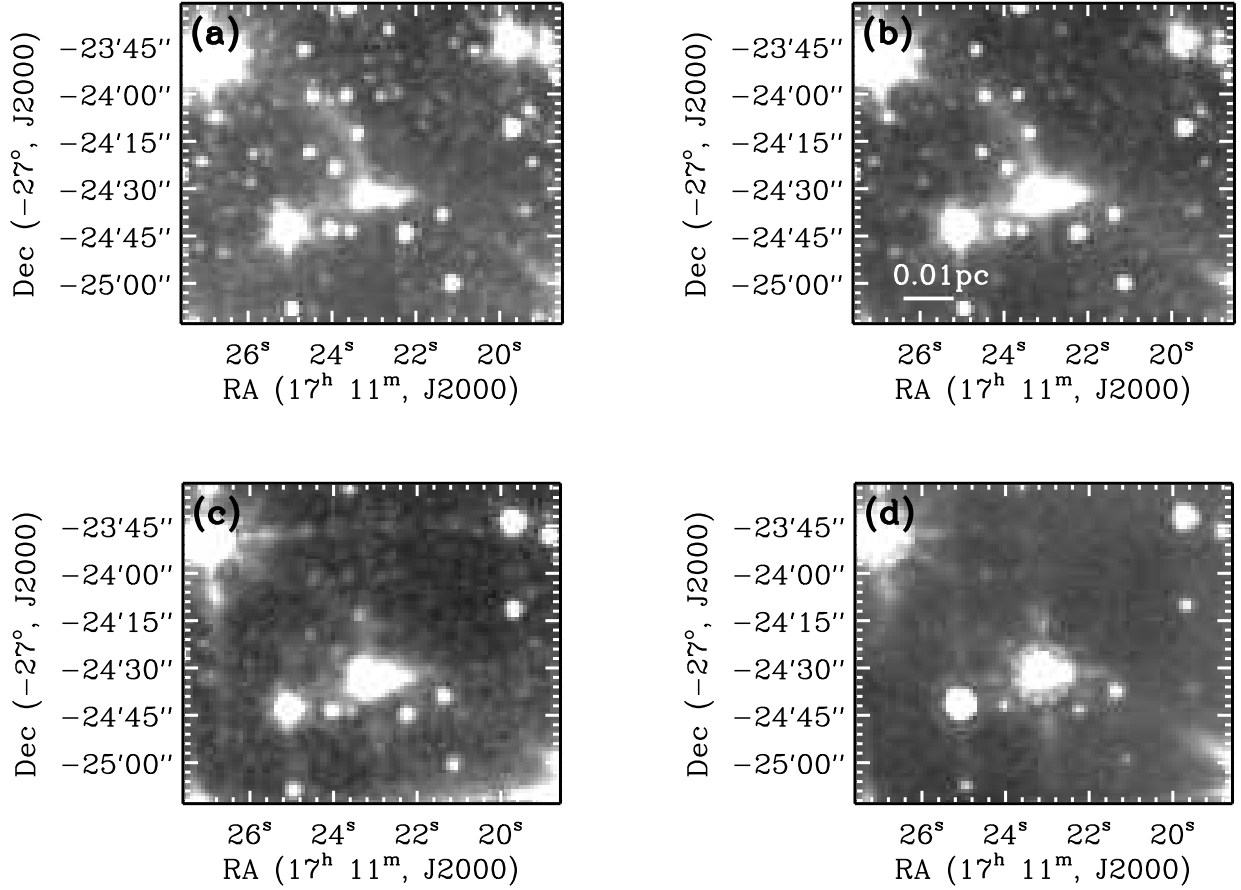


Fig. 5.— Close-up of the Class 0/I source 11 = 2MASS171123, closest to center, through the 4 IRAC bands: *a*) 3.6  $\mu\text{m}$ , *b*) 4.5  $\mu\text{m}$ , *c*) 5.8  $\mu\text{m}$ , *d*) 8.0  $\mu\text{m}$ . Image arcs visible at 3.6 and 4.5  $\mu\text{m}$  may trace an outflow cavity in scattered light. Scale bar plotted in (*b*) is for assumed distance of  $d = 130$  pc.

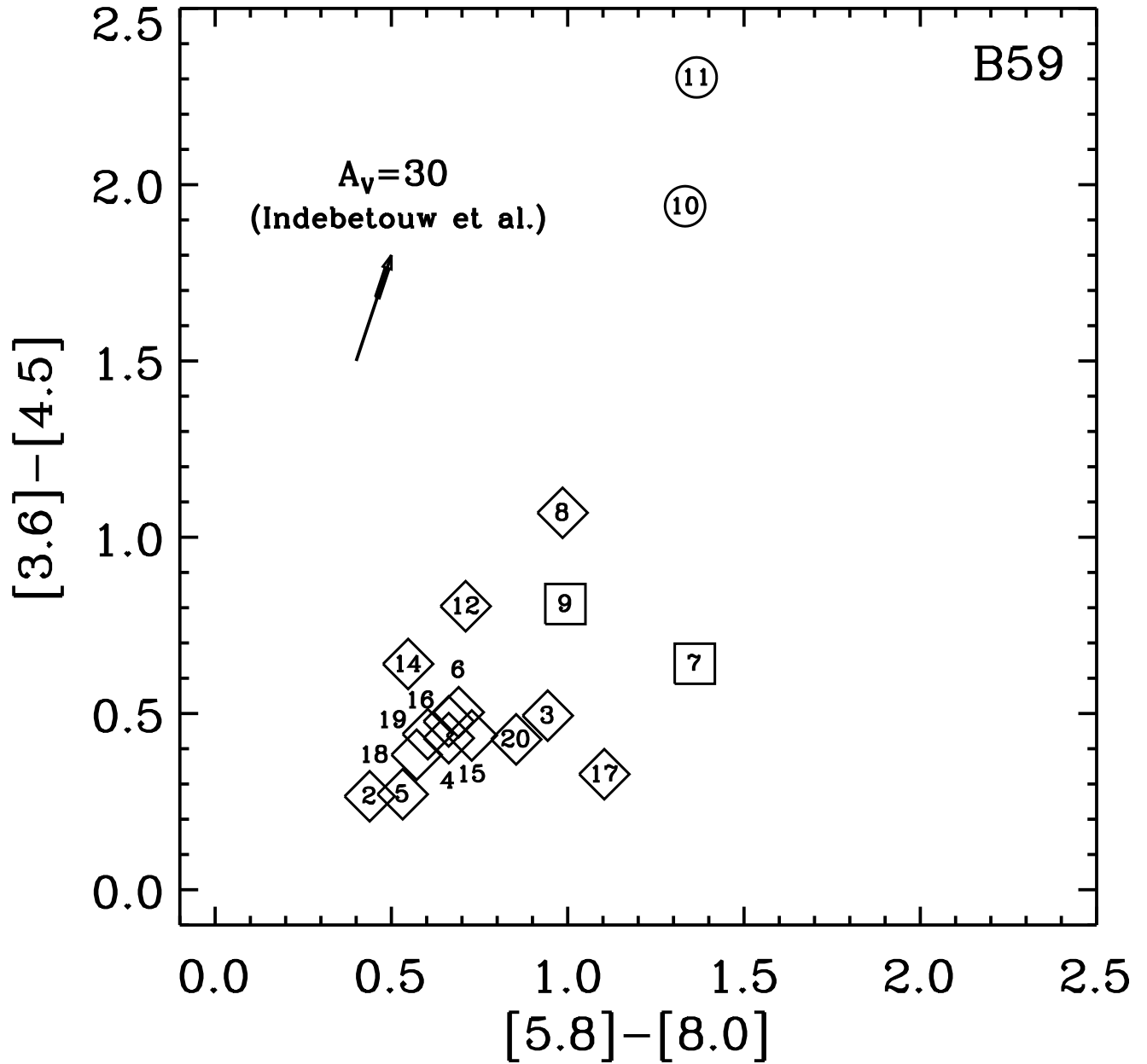


Fig. 6.— IRAC color-color diagram, as observed, of candidate young stars in B59 with source numbers from Table 1. Young star IR spectral classes, after correction for extinction (where possible) are indicated with the following symbols: Class I (*circle*), Flat (*square*), and Class II (*diamond*). The reddening arrow shows the adopted extinction law (Indebetouw et al., 2005) for  $A_V \approx 30$  mags (see text).

Table 1. Candidate Young Stars in B59<sup>a</sup>

No.	2MASS Name	Other ID	RA(J2000)	DEC(J2000)	J	H	K <sub>s</sub>	A <sub>V</sub> (JHK) <sup>g</sup>	A <sub>V</sub> (Map) <sup>h</sup>	Comments
1	J17110392-2722551	LkH $\alpha$ 346 NW	17 11 03.91	-27 22 55.2	10.46 (0.03)	8.99 (0.03)	7.76 (0.02)	2.6 (1.7)	10.0 (0.6)	Triple <sup>b</sup> IRAS17079-2719
2	J17110411-2722593	LkH $\alpha$ 346 SE	17 11 04.12	-27 22 59.3	9.75 (0.03)	8.79 (0.04)	8.05 (0.03)	0.0 (1.5)	9.9 (0.6)	
3	J17111182-2726547	...	17 11 11.82	-27 26 55.0	14.09 (0.02)	12.62 (0.03)	11.76 (0.02)	5.6 (1.4)	19.2 (1.9)	
4	J17111445-2726543	...	17 11 14.45	-27 26 54.4	11.62 (0.02)	10.42 (0.02)	9.63 (0.02)	2.7 (1.3)	22.4 (2.8)	
5	J17111626-2720287	...	17 11 16.27	-27 20 28.8	11.23 (0.02)	9.70 (0.02)	9.07 (0.02)	8.3 (0.8)	7.3 (0.3)	
6	J17111631-2725144	KW 2	17 11 16.32	-27 25 14.6	10.58 (0.02)	9.37 (0.02)	8.75 (0.02)	4.2 (1.1)	14.7 (2.3)	H $\alpha$ <sup>c</sup>
7	J17111726-2725081	IRAS17081-2721	17 11 17.28	-27 25 08.2	13.61 (0.04)	10.82 (0.04)	8.77 (0.03)	13.0 (1.8)	15.7 (2.5)	
8	J17111827-2725491	...	17 11 18.13	-27 25 49.3	>18.4	15.12 (0.08)	11.95 (0.03)	44 (8)	25.3 (6.2)	
9	J17112153-2727417	IRAS17082-2724	17 11 21.50	-27 27 42.3	12.74 (0.02)	10.57 (0.02)	8.98 (0.02)	8.7 (1.7)	26.9 (5.0)	
10	...	...	17 11 22.10	-27 26 2.0	...	...	...	...	46.1 (20.0)	
11	J17112317-2724315	...	17 11 23.18	-27 24 31.5	>18.8	>17.8	15.08 (0.14)	...	25.7 (5.7)	Prob. MMS1 <sup>d</sup>
12	J17112508-2724425	...	17 11 25.08	-27 24 42.7	16.52 (0.11)	13.61 (0.03)	11.57 (0.02)	14.7 (2.2)	27.2 (5.7)	

Table 1—Continued

No.	2MASS Name	Other ID	RA(J2000)	DEC(J2000)	J	H	K <sub>s</sub>	A <sub>V</sub> (JHK) <sup>g</sup>	A <sub>V</sub> (Map) <sup>h</sup>	Comments
13	J17112701-2723485	B59-1	17 11 26.95	-27 23 48.4	11.88 (0.04)	10.14 (0.04)	9.08 (0.03)	7.5 (1.5)	24.4 (2.4)	Triple <sup>e</sup>
14	J17112729-2725283	...	17 11 27.06	-27 25 29.5	13.17 (0.02)	10.65 (0.02)	9.11 (0.02)	13.7 (1.3)	33.2 (8.6)	
15	J17112942-2725367	...	17 11 29.31	-27 25 36.3	13.28 (0.02)	11.74 (0.02)	10.70 (0.02)	5.1 (1.3)	23.6 (3.7)	
16	J17113036-2726292	...	17 11 30.29	-27 26 29.3	11.91 (0.03)	10.00 (0.02)	8.89 (0.02)	9.3 (1.4)	20.7 (2.7)	
17	J17114099-2718368	IRAS17085-2715	17 11 40.99	-27 18 37.0	10.64 (0.02)	8.75 (0.04)	7.54 (0.02)	8.2 (1.4)	8.4 (0.8)	
18	J17114182-2725477	B59-2	17 11 41.73	-27 25 50.3	11.3 (0.2)	10.4 (0.2)	10.1 (0.2)	4.1 (4.3)	11.7 (0.6)	Double <sup>f</sup>
19	J17114315-2730584	...	17 11 43.16	-27 30 58.6	14.09 (0.03)	12.75 (0.03)	11.91 (0.03)	4.1 (1.4)	10.1 (1.2)	
20	J17120020-2720180	LkHα 347	17 12 0.20	-27 20 18.1	10.54 (0.02)	9.64 (0.03)	9.17 (0.02)	1.4 (1.1)	6.9 (0.8)	

Note. —

<sup>a</sup> Within field covered by both IRAC and MIPS 24  $\mu\text{m}$ . Uncertainties in parentheses. Adopted flux zero points for the 2MASS J, H, and K<sub>s</sub> filters are 1594, 1024, and 667 Jy, respectively.

<sup>b</sup> LkHα 346 SE is labelled the primary (A) and has a tertiary companion (C) according to Chelli et al. (1995). The AC pair is unresolved by *Spitzer*. LkHα 346 NW, or (B), is the brighter infrared source.

<sup>c</sup> Hα emission (Kohoutek & Wehmeyer 2003).

<sup>d</sup> Probably MMS1 of Reipurth et al. (1996). See text.

<sup>e</sup> The source is triple according to Koresko (2002). The brighter source is the primary (plus tertiary), for which the position and fluxes are given.

<sup>f</sup> The source is double (Reipurth & Zinnecker 1993), possibly triple (Koresko 2002). The brighter mid-infrared source is the secondary, for which the position and fluxes are given. The JHK fluxes are from Koresko (2002).

<sup>g</sup> Extinction from dereddening to T Tauri JHK<sub>s</sub> locus.

<sup>h</sup> Cloud extinction from background stars.

Table 2. Spitzer Fluxes (mJy) of Candidate Young Stars in B59<sup>a</sup>

No.	Other ID	3.6	4.5	5.8	8.0	24	70	$\alpha^b$	IR Class <sup>c</sup>	$\alpha^d$	IR Class <sup>e</sup>	$L_{\text{bol}}(L_{\odot})^f$
1	LkH $\alpha$ 346 NW	699 (9)	881 (13)	...	1440 (25)	6320 (1260)	8490 (40)	-0.22	Flat	-0.35 <sup>g</sup>	Flat	>1.6
2	LkH $\alpha$ 346 SE	218 (3)	180 (2)	174 (4)	141 (1)	...	...	-1.81	II	-1.81	II	0.50 (0.11)
3	...	15.5 (0.2)	15.8 (0.1)	16.2 (0.1)	20.9 (0.1)	94.5 (0.4)	110 (5)	-0.64	II	-0.92	II	0.14 (0.08)
4	...	90.1 (1.1)	86.6 (0.7)	78.4 (0.5)	78.1 (0.4)	155 (1)	210 (6)	-1.14	II	-1.27	II	0.26 (0.09)
5	...	106 (1)	88.0 (1)	77.1 (0.5)	68.1 (0.6)	45.5 (0.3)	<100	-1.64	II	-2.04	II	0.98 (0.09)
6	KW 2	211 (3)	217 (3)	223 (2)	228 (3)	...	...	-0.94	II	-1.14	II	0.93 (0.13)
7	IRAS17081-2721	609 (8)	711 (16)	929 (11)	1760 (24)	9200 (1840)	10100 (50)	0.66	I	0.02	Flat	>2.7
8	...	58.9 (0.7)	102 (2)	126 (1)	169 (2)	412 (3)	1440 (10)	1.11	I	-1.04	II	1.4 (1.0)
9	IRAS17082-2724	310 (4)	423 (6)	601 (6)	812 (9)	1540 (17)	2070 (10)	0.21	Flat	-0.22	Flat	>0.86
10	...	3.2 (0.1)	12.5 (0.1)	21.6 (0.2)	39.9 (0.2)	1710 (29)	9190 (30)	2.16 <sup>g</sup>	I	...	...	0.63 (0.13)
11	...	6.4 (0.2)	34.3 (0.8)	83.0 (0.8)	158.0 (1.8)	4715 (940)	42100 (8400)	3.29	0/I	...	...	2.2 (0.3)
12	...	34.2 (0.3)	46.4 (0.4)	46.2 (0.3)	48.1 (0.3)	88.7 (0.5)	...	-0.13	Flat	-0.85	II	0.16 (0.09)

Table 2—Continued

No.	Other ID	3.6	4.5	5.8	8.0	24	70	$\alpha^b$	IR Class <sup>c</sup>	$\alpha^d$	IR Class <sup>e</sup>	$L_{\text{bol}}(L_{\odot})^f$
13	B59-1	146 (2)	178 (2)	...	235 (3)	831 (5)	1780 (10)	-0.68	II	-1.04	II	0.53 (0.13)
14	...	222 (3)	259 (3)	250 (3)	224 (3)	455 (3)	710 (7)	-0.69	II	-1.36	II	0.81 (0.16)
15	...	37.5 (0.3)	36.3 (0.3)	36.2 (0.3)	38.3 (0.3)	104 (1)	246 (4)	-0.93	II	-1.18	II	0.17 (0.09)
16	...	243 (3)	244 (3)	254 (2)	253 (3)	150 (1)	1310 (6)	-0.76	II	-1.21	II	0.74 (0.16)
17	IRAS17085-2715	471 (7)	412 (6)	450 (4)	670 (8)	1050 (9)	...	-0.97	II	-1.37	II	1.81 (0.37)
18	B59-2	74.1 (0.8)	68.2 (0.8)	51.2 (0.3)	46.9 (0.4)	56.5 (0.4)	<100	-1.57 <sup>h</sup>	II	-1.67 <sup>h</sup>	II	0.1-0.9
19	...	14.0 (0.1)	13.6 (0.2)	12.3 (0.1)	11.6 (0.1)	21.6 (0.2)	<100	-0.99	II	-1.19	II	0.13 (0.08)
20	LkH $\alpha$ 347	119 (2)	114 (2)	101 (1)	120 (1)	213 (1)	...	-1.13	II	-1.20	II	0.36 (0.10)

Note. —

<sup>a</sup> Within field covered by both IRAC and MIPS 24  $\mu\text{m}$ .  $1\sigma$  errors (in parentheses) are from photometric fitting and do not include absolute flux error (see text). A blank entry indicates no useful value due to confusion with nearby source(s), or due to lack of data.

<sup>b</sup> Spectral index  $d\log(\lambda F_{\lambda})/d\log(\lambda)$  with endpoints at 2.2 and 8.0  $\mu\text{m}$  uncorrected for extinction, unless different endpoint wavelengths in  $\mu\text{m}$  are noted.

<sup>c</sup> IR spectral class.



<sup>d</sup> Same as b after correction for extinction.

<sup>e</sup> Same as c after correction for extinction.

<sup>f</sup> Bolometric luminosity (or lower limit) estimated as discussed in text. Uncertainties (in parentheses) do not include uncertainty in distance.

<sup>g</sup> On border of Flat and Class II, but longer wavelengths indicate Flat.

<sup>h</sup> Spectral index is from 3.6 to 8.0  $\mu\text{m}$ .